Direct Imaging of Exoplanets: Science & Techniques
Proceedings IAU Colloquium No. 200, 2005
C. Aime and F. Vakili, eds.

doi:10.1017/S1743921306009604

Apodized Pupil Lyot Coronagraphs: Concepts and application to the Gemini Planet Imager

Rémi Soummer[1]†, Claude Aime[2], André Ferrari[2], Anand Sivaramakrishnan[1], Ben R. Oppenheimer[1], Russell Makidon [3], and Bruce Macintosh [4]

[1]American Museum of Natural History, 79th St at Central Park West, New York, USA
email: rsoummer@amnh.org, anand@amnh.org, bro@amnh.org

[2]Laboratoire Universitaire d'Astrophysique de Nice, Parc Valrose, Nice, France
email: Claude.Aime@unice.fr, Andre.Ferrari@unice.fr

[3]Space Telescope Science Institute, 3700 San Martin Drive, Baltimore, USA
email: makidon@stsci.edu

[4]Lawrence Livermore National Laboratory, 7000 East Avenue, Livermore, USA
email:bmac@igpp.ucllnl.org

Abstract. This paper summarizes the general theory and properties for Apodized Pupil Lyot Coronagraphs which consist of a classical hard-edged Lyot coronagraph with an upstream pupil apodization. The ideal apodization function can be determined from an integral eigenvalue problem which solutions are prolate spheroidal functions. Solutions exist for any geometrty, including rectangular, circular, or elliptical. Formal solutions can be extended to the case of arbitrary apertures, using generalized prolate spheroidal functions for centrally obstructed apertures, spiders, or segmented telescopes. The properties of these coronagraphs enable the possibility of multiple stage coronagraphy and achromatization. The new instrument Gemini Planet Imager (GPI) will include such a coronagraph.

Keywords. instrumentation: high angular resolution, instrumentation: adaptive optics.

1. Introduction

Direct imaging and spectroscopy of extrasolar planets is an exciting and ambitious goal, which requires advanced starlight cancellation techniques, including coronagraphy. The Gemini Planet Imager (GPI), Macintosh *et al.* (2004), will aim at imaging and spectroscopy of Extrasolar Giant Planets (EGP). Classical methods like the Lyot Coronagraph are not efficient enough to reach the necessary contrast for this science goal, Burrows *et al.* (2004), and more advanced techniques have to be considered. The Apodized Pupil Lyot Coronagraph has been selected for this new instrument. We summarize in this communication the theory and properties of these coronagraphs detailed by Aime *et al.* (2001); Aime *et al.* (2002); Soummer *et al.* (2003); Soummer (2005), we also include the possibility of multiple stage APLC, Aime & Soummer (2004), achromatization, Aime (2005) and discuss their fabrication.

† Michelson Fellow

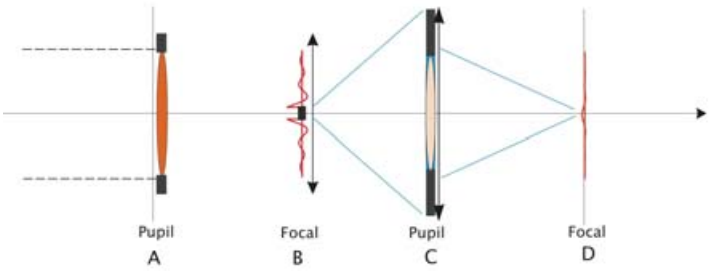

Figure 1. The basic layout of an APLC is similar to a classical Lyot coronagraph, but adding an upstream apodized pupil in Plane A. A hard hedged focal maks is set in the focal plane B, and a Lyot stop *identical* to the entrance pupil shape in plane C. A remarquable difference between APLC and classical Lyot is that APLCs don't require to undersize the Lyot stop.

2. Apodized Pupil Lyot Coronagraphy with arbitrary aperture shapes

Following the notation of Aime *et al.* (2002) and Soummer *et al.* (2003), we briefly recall the general formalism of coronagraphy with apodized pupils. The general layout of an APLC is recalled in Fig. 1, and is similar to a classical Lyot coronagraph, but using an upstream pupil apodization. The telescope aperture function with the position vector $\mathbf{r}$ is denoted by $P(\mathbf{r})$, and $\Phi(\mathbf{r})$ is the apodizer transmission (1 without apodization). At the entrance aperture, the wavefront amplitude is:

$$\Psi_A(\mathbf{r}) = P(\mathbf{r})\,\Phi(\mathbf{r}). \tag{2.1}$$

A mask of transmission $1 - \epsilon M(\mathbf{r})$ is placed in the focal plane. M is a function that describes the mask shape, equal to 1 inside the coronagraphic mask and 0 outside ($\epsilon = 1$ for Lyot and $\epsilon = 2$ for Roddier).

At the Lyot stop plane, the wavefront is then:

$$\Psi_C(\mathbf{r}) = P(\mathbf{r})\,\Phi(\mathbf{r}) - \frac{\epsilon}{\lambda^2 f^2}\int_P \Phi(\mathbf{u})\,\widehat{M}\left(\frac{\mathbf{r}-\mathbf{u}}{\lambda f}\right)\mathrm{d}\mathbf{u}, \tag{2.2}$$

where $\widehat{\ }$ is the Fourier Transform. This general relation is valid for any arbitrary aperture shape (rectangular, circular or elliptical, with or without central obstruction and secondary mirror supports), and any mask shape, Soummer (2005). In this equation we assume that the focal lengths of the successive optical systems are identical (if not, an appropriate change of variables leads to the same result), we re-orientate the axis in the opposite direction and omit the -1 proportionality factor for better readability. The formal problem is to find the mask $M(\mathbf{r})$ and the apodizer $\Phi(\mathbf{r})$ that provide the best cancellation possible inside the Lyot stop, identical to the entrance pupil in this case.

A perfect solution (total extinction) is obtained if the wave diffracted by the mask (the convolution integral) is equal to the initial pupil amplitude. In more mathematical terms, this means that $\Phi(\mathbf{r})$ must be the eigenfunction of the convolution integral in Eq.2.2. This problem is equivalent to the generalization of the uncertainty principle, Papoulis (1968), with the search of band-limited functions having the maximum encircled energy within a given spatial domain. In coronagraphic terms, the solution is the pupil apodization which produces the most concentrated star light behind a given focal plane mask (and thus blocked). This formal problem has been solved analytically for rectangular and circular unobstructed apertures, Aime *et al.* (2001), Aime *et al.* (2002), Soummer *et al.* (2003), involving linear and circular prolate functions, Slepian & Pollak (1961), Frieden (1971), Papoulis (1981). In the general case, formal solutions exist, Slepian (1964), Slepian

https://doi.org/10.1017/S1743921306009604 Published online by Cambridge University Press

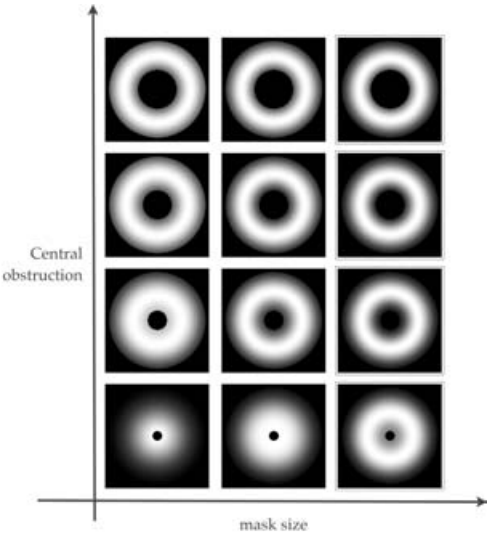

Figure 2. A given telescope geometry defines an integral eigenvalue problem in which for any mask size (eigenvalue), an apodization can be computed (eigenfunction). This figure illustrates the apodization that can be obtained for a few telescope geometries varying the size of the central obstruction (y-axis), and as a function of the maks size (x-axis).

(1965), Papoulis (1968), Soummer (2005), and are the eigenfunction of the 2-D integral equation:

$$\int_P \Phi(\mathbf{t})\, \widehat{M}(\mathbf{r}-\mathbf{t})\, \mathrm{d}\mathbf{t} = \Lambda\, \Phi(\mathbf{r}). \tag{2.3}$$

The solution $\Phi(\mathbf{r})$ corresponds to the largest eigenvalue Λ_0, and to the maximum encircled energy behind the focal plane mask $e = \Lambda_0$. The mask size is directly related to the eigenvalue, and therefore, for a given mask size, a unique apodization function exists. In Fig. 2, we show the apodizer as a function of the mask size and for a few telescope geometries, varying the obstruction size.

The expression of the residual wavefront inside the Lyot stop for circular and rectangular geometries is the same for the general case:

$$\Psi_C^+(\mathbf{r}) = \Psi_A(\mathbf{r})(1-\epsilon\,\Lambda_0), \tag{2.4}$$

(the $^+$ signifies this is just after the Lyot stop). As detailed in previous work, and illustrated in Fig. 3, the wavefront is therefore simply proportional to the initial apodization function, with a constant of proportionality $(1-\epsilon\,\Lambda_0)$.

3. Mutiple Stage APLCs and achromatization

3.1. *Multiple Stage*

As described above, the Lyot stop wave amplitude is proportional to the entrance apodized pupil amplitude. This enables the possibility for multiple stage coronagraphs described by Aime *et al.* (2002) and Aime & Soummer (2004) (Fig. 4), which could help ambitious projects such as TPF to reach their required extinction. A multiple stage APLC only requires a single apodizer in the entrance pupil. The Lyot stop plane is naturally apodized, and can be used as the entrance pupil of a second coronagraphic stage without further loss of throughput due to apodization (Fig. 4). Eq.2.4 can be straightforwardly

https://doi.org/10.1017/S1743921306009604 Published online by Cambridge University Press

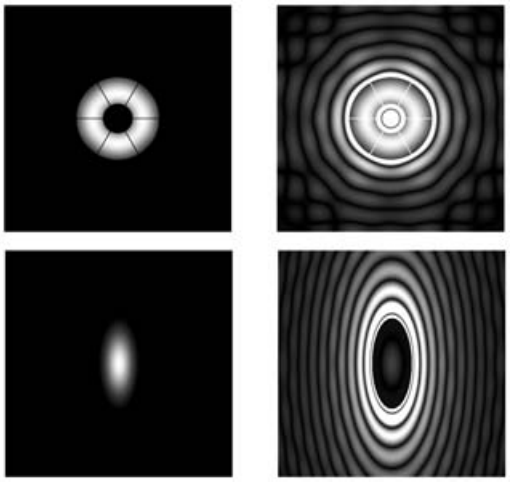

Figure 3. Examples of APLCs for two geometries: the Overwhelmingly Large Telescope (OWL) (top) and the Terrestrial Planet Finder (TPF) (bottom). The left images correspond to the entrance pupil apodization, and the right images to the Lyot stop plane (plane C) wave amplitude. The field amplitude inside the aperture domain is proportional to the initial entrance pupil apodization, since the apodizer is the eigenfunction of the problem. This property enables the possibility of multiple stage APLCs for any telescope geometry.

extrapolated to the multiple stage case, and the residual amplitude in the second Lyot stop plane (plane E of Fig. 4) is:

$$\Psi_E^+(\mathbf{r}) = \Psi_A(\mathbf{r})(1 - \epsilon\,\Lambda_0)^2. \tag{3.1}$$

In principle, several identical coronagraphs can be used in a cascading mode. Each coronagraph produces the same reduction factor of the star light. Denoting Q the efficiency of one coronagraph, the efficiency of N cascaded coronagraph should be Q^N.

3.2. *Achromatization*

The main limitation of APLCs comes from the chromaticity due to the PSF size, which is proportional to the wavelength. In the simple case of a focal plane mask made by means of a hole in a mirror, its size is identical at all wavelengths. Therefore, the mask is too large at short wavelengths, and too small at long wavelengths, which translates into a leak through the coronagraphs. Specific designs can accommodate these limitations, such as the Dual-Zone coronagraph, Soummer *et al.* (2003). In the case of APLCs, a mitigation of these chromatic effects can be obtained by optimizing the mask size for an effective wavelength with optimum efficiency over the actual bandpass, Soummer (2005).

For a given physical mask, each wavelength corresponds to a different mask size in resolution element units (λ/D). Therefore, it is possible to compute the required apodization as a function of the wavelength since an apodization corresponds to a given mask size, Aime (2005).

A perfect achromatic solution can be obtained with an apodizer producing this variable apodization with wavelength. In this case the result is close to that of an achromatic APLC at the shortest wavelength of the bandpass. Aime (2005) has proposed an interferometric method to produce such a wavelength-dependent apodizer, using dispersive optics in the arms of an interferometer. Interferometric methods to produce apodizers have been studied by Aime *et al.* (2001). The results of a laboratory experiment validating this concept is given in this volume by El Azhari *et al.* (2005).

https://doi.org/10.1017/S1743921306009604 Published online by Cambridge University Press

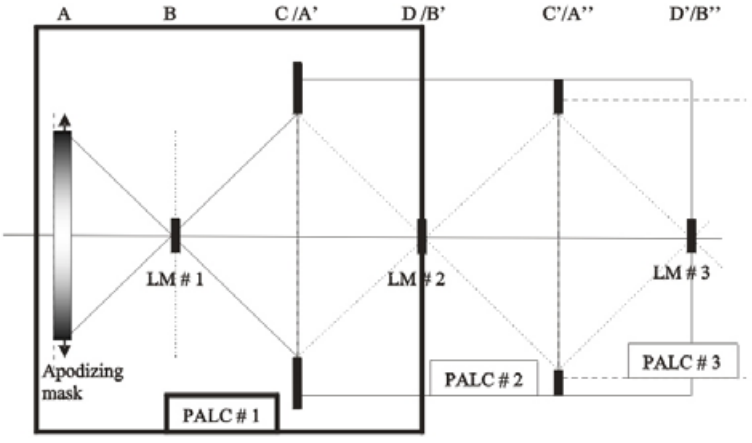

Figure 4. Schematic representation of a multiple-Lyot coronagraph. The light goes from left to right. The first square box, entitled $PALC\sharp 1$, for Prolate Apodized Lyot Coronagraph number 1 is the classical Lyot coronagraph with entrance aperture apodization. The successive planes are denoted A, B, C and D. A is the entrance aperture (or image of the aperture) with the prolate apodization, B denotes the focal plane with the first Lyot mask ($LM\sharp 1$), C is the image of the aperture with the Lyot stop, and D is the image of the focal plane after the coronagraph (D is the final focal plane in the case of a classical apodized coronagraph. The second stage of the coronagraph consists of planes A', B', C' and D'. Planes A' and B' merge respectively with plane C and D. A Lyot mask, identical to the one in plane B, is set in plane B' (or D). A Lyot stop in plane C', identical to the one in plane C, completes the second stage. The image is observed in plane D'. The coronagraph $PALC\sharp 2$ produces the same starlight rejection as the $PALC\sharp 1$, because the amplitude in C/A' is proportional to the amplitude in A without the need of another apodizer. For a perfect system, this rejection is obtained without loss of useful light for the planet. The first part of a third coronagraph ($PALC\sharp 3$) is drawn in the figure.

A more simple method, though which might not be able to provide perfect achromatization, is to manufacture an apodizer using an absorbing material which approximates the required wavelength variation. First tests using High Energy Electron Beam Sensitive glass (HEBS glass) have shown that this material improves the performance of the APLC in the infrared by a factor of 5. This preliminary result can be further improved by adjusting the chromaticity of the material itself (Soummer etal. in preparation).

4. Application to the Gemini ExAOC

Thanks to the recent results on the understanding of the theory of APLCs in the presence of spiders and central obstruction, Soummer (2005), Sivaramakrishnan & Lloyd (2005), and recent lab results on the fabrication of apodizers for the infrared using HEBS glass, the APLC has been selected as the baseline concept for the Gemini Planet Imager. As compared to a classical Lyot for similar mask size ($4.5\lambda/D$ to $5..5\lambda/D$) and because APLCs do not require Lyot Stop size reduction, both the coronagraphic rejection and the throughput can be improved compared to a classical Lyot (Fig. 5). This instrument will include an Extreme Adaptive Optics system, an APLC, an Integral Field Spectrograph, and an active calibration system. The predicted dynamic range limits at the 5-σ level (Fig. 6) are compatible with the main goal of detecting Extrasolar Giant Planets around nearby stars.

https://doi.org/10.1017/S1743921306009604 Published online by Cambridge University Press

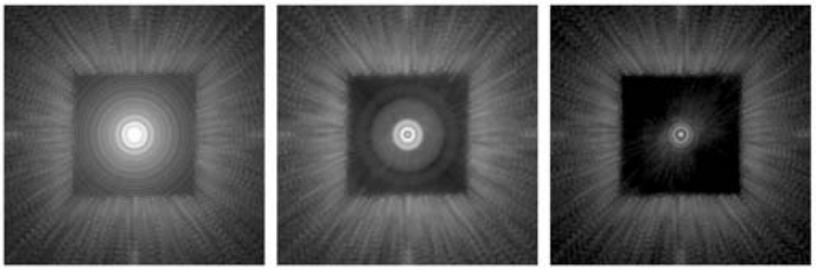

Figure 5. From Left to right: AO-corrected PSF, Lyot Coronagraphic PSF, APLC coronagraphic PSF. The square dark region corresponds to the area of the field corrected by the spatially filtered AO system. The halo clearing is improved over the classical Lyot, using the same mask size ($4.7\lambda/D$). Thanks to the properties of the APLC, its overall transmission (55%) is higher than that of a comparable classical Lyot (50%), and for a better rejection.

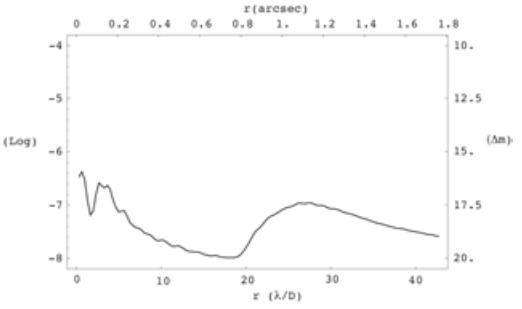

Figure 6. Dynamic range simulation including speckle and photon noise for a 7th magnitude star, in 1000s in Hband for the Gemini ExAOC. This type of dynamic range plots can be readily used in Monte-Carlo simulations to study the completeness of the observations.

Acknowledgements

Rémi Soummer is supported by a Michelson Fellowship, under contract with the Jet Propulsion Laboratory funded by NASA. JPL is managed for NASA by the California Institute of Technology.

References

Aime, C. 2005, *PASP*, 117, 1112
Aime, C. & Soummer, R. 2004, *proc. SPIE*, 5490, 456
Aime, C., Soummer, R., & Ferrari, A. 2001, *A&A*, 379, 697
Aime, C., Soummer, R., & Ferrari, A. 2002, *A&A*, 389, 334
Burrows, A., Sudarsky, D., & Hubeny, I. 2004, *ApJ*, 609, 407
El Azhari, Y., Azagrouze, O., Martin, F, Soummer, R., & Aime, C. 2005, *Proc. IAU Colloquium No. 200*, 609, 407
Frieden, B. R. 1971, *Progress in Optics*, ed. E. Wolf, Vol. 9
Macintosh, B. A., *et al.* 2004, *Proc. SPIE*, 5490, 359
Papoulis, A. 1968, *Systems and transforms with applications in optics* (McGraw-Hill Series in System Science (reprint 1981))
Papoulis, A. 1981, *Signal Analysis*, ed. M. G. Hill
Sivaramakrishnan, A. & Lloyd, J. P. 2005, *ApJ*, 633, 528
Slepian, D. 1964, *Bell Syst. Tech. J.*, 43, 3009
Slepian, D. 1965, *J. Opt. Soc. Am.*, 55; no.9
Slepian, D. & Pollak, H. O. 1961, *Bell Syst. Tech. J.*, 40, 43
Soummer, R., Aime, C., & Falloon, P.E. 2003, *A&A*, 397, 1161
Soummer, R., Dohlen, K., & Aime, C. 2003, *A&A*, 403, 369
Soummer 2005, *ApJ*, 618, 161